PROCEEDINGS OF SPIE

SPIEDigitalLibrary.org/conference-proceedings-of-spie

Vortex phase masks of topological charge 4 and higher with diamond subwavelength gratings

König, Lorenzo, Absil, Olivier, Delacroix, Christian, Lobet, Michaël, Karlsson, Mikael, et al.

Lorenzo König, Olivier Absil, Christian Delacroix, Michaël Lobet, Mikael Karlsson, Ernesto Vargas Catalán, Gilles Orban de Xivry, Jérôme Loicq, Serge Habraken, "Vortex phase masks of topological charge 4 and higher with diamond subwavelength gratings," Proc. SPIE 11451, Advances in Optical and Mechanical Technologies for Telescopes and Instrumentation IV, 1145144 (13 December 2020); doi: 10.1117/12.2576166

SPIE.

Event: SPIE Astronomical Telescopes + Instrumentation, 2020, Online Only

Vortex Phase Masks of Topological Charge 4 and higher with Diamond Subwavelength Gratings

Lorenzo König[a], Olivier Absil[a], Christian Delacroix[a], Michaël Lobet[b], Mikael Karlsson[c], Ernesto Vargas Catalán[c], Gilles Orban de Xivry[a], Jérôme Loicq[b], and Serge Habraken[a]

[a]STAR Institute, Université de Liège, Allée du Six Août 19C, B-4000 Liège, Belgium
[b]Centre Spatial de Liège, Université de Liège, Avenue du Pré-Aily, B-4031 Angleur, Belgium
[c]Department of Engineering Sciences, The Angstrom Laboratory, Uppsala University, P.O. Box 534, SE-751 21 Uppsala, Sweden

ABSTRACT

High contrast imaging at small inner working angles can be achieved using a vector vortex coronagraph in the focal plane of the telescope providing a helical phase ramp with a singularity at its center. The form birefringence of full-diamond subwavelength gratings has proven to be well suited to manufacture such vortex phase masks for coronagraphic applications (Subwavelength Grating Vortex Coronagraph, SGVC). In the past years our group has developed and manufactured SGVCs of topological charge 2 (Annular Groove Phase Mask, AGPM) made of a concentric diamond subwavelength grating. For future applications including ELT-class telescopes in the near- to mid-infrared that will partly resolve nearby stars, it is however useful to increase the topological charge of the vortex. After shortly reviewing our previous attempts at optimizing the grating structure for SGVC of charge 4, we present the first laboratory results obtained with such devices. We then introduce and discuss more realistic simulations compared to prior studies using finite-difference time-domain methods. The quality of the simulation results obtained with the open source software MEEP for an AGPM is shown to be appropriate for developing and assessing the performance of future vortex phase masks. We therefore perform updated simulations for SGVC of charge 4 including various designs with straight and curved grating lines. We conclude with a perspective on the potential of metasurfaces and their applications to design novel vortex coronagraphs based on subwavelength structures.

Keywords: extrasolar planet, high contrast imaging, small inner working angle, vector vortex coronagraph, subwavelength grating, phase mask, metasurfaces

1. INTRODUCTION

In the past years, the number of exoplanet discoveries has grown rapidly reaching more than 4000 as of today.[1] One key of studying these planets and to characterize their atmospheres is direct imaging. A high contrast coronagraph with small inner working angle is needed to provide the means of direct imaging of Earth-sized planets. A vector vortex coronagraph consisting of a pure phase mask is able to send all the light of an on-axis source outside the telescope pupil by destructive interference where it is blocked by a Lyot Stop. In this context, our group has developed the Annular Groove Phase Mask (AGPM),[2] using the form birefringence of subwavelength gratings. This allows us to achieve a broadband performance of the AGPM of up to 50% bandwidth. Several AGPMs have been designed and manufactured since then and installed on major instruments (VISIR,[3] NACO,[4,5] LMIRCam[6]) providing excellent results. However, it seems mandatory to increase the so-called topological charge of the vortex to make the coronagraph more resilient to low-order aberrations and to partly resolved stars, which will be the case for future ELT-class telescopes.

After shortly reviewing the concept of vortex phase masks of topological charge 4 made so far[7] (Section 2), we present first laboratory results obtained with two SGVC4 patterns showing encouraging first results (Section 3). We then discuss simulation results using a finite-difference time-domain method (FDTD) for different SGVC4 patterns and challenges encountered with those discretized designs (Section 4). We conclude with a perspective on full-metasurface structures to create the phase ramp (Section 5).

Send correspondence to: lorenzo.konig@uliege.be

Advances in Optical and Mechanical Technologies for Telescopes and Instrumentation IV, edited by Ramón Navarro, Roland Geyl, Proc. of SPIE Vol. 11451, 1145144
 · doi: 10.1117/12.2576166

2. CONTEXT

In the past 10 years we have successfully designed and manufactured several AGPMs and installed them on major telescopes all around the globe. We use the artificial birefringence of subwavelength gratings to induce a helical phase ramp and create an optical vortex sending all light outside the telescope pupil where it is intercepted by a Lyot Stop (for details see Ref. 2). For the upcoming ELT class telescopes in the near future, it is however useful to increase the topological charge of the vortex to be more resilient to low-order aberrations and to account for partly resolved stars. While a higher topological charge gradually removes low order aberrations,[8] it comes at a drawback of a larger inner working angle (1.6 λ/D for a charge-4 vortex compared to 0.9 λ/D for charge-2, see figure 1).

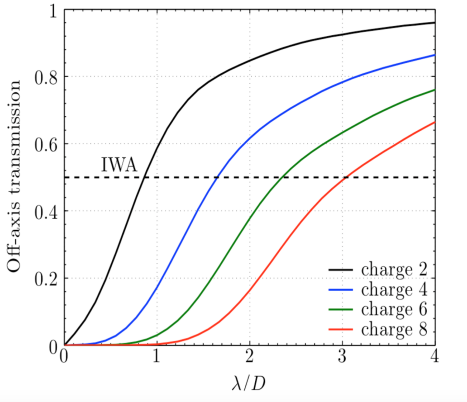

Figure 1. Off-axis transmission of vortex masks of different topological charge.

For the AGPM, we have used a continuous pattern of concentric subwavelength gratings. For higher topological charges, the pattern becomes more complicated and impossible to manufacture (see figure 2). To mitigate this problem, we suggested the segmentation of the grating pattern.[7] Two main patterns have been proposed, one using equally spaced segments with straight lines and one using curved lines with segments of variable size. We now propose a third hybrid pattern combining the strength of both main patterns. These patterns are simulated using rigorous FDTD simulation tools (see section 4).

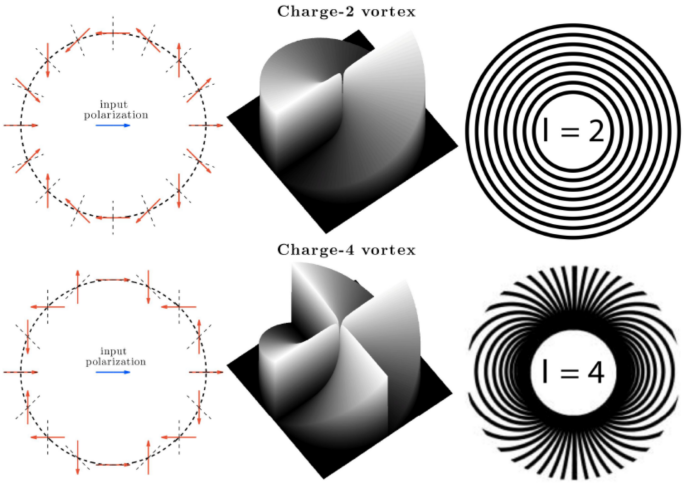

Figure 2. Working principle and theoretical pattern for the charge 4 vortex using subwavelength gratings.[7]

3. LABORATORY RESULTS

Three SGVC4 for the L band (3.5 µm – 4.1 µm) have been manufactured in the past years: one eight-segment mask, and two identical 32-segment masks, all having a straight lines pattern (see figure 3). The manufacturing process is detailed in Ref. 9. An anti-reflective grating is etched on the backside of the masks to reduce internal reflections. We tested these masks on the dedicated test bench VODCA (Vortex Optical Demonstrator for Coronagraphic Analysis).[10,11]

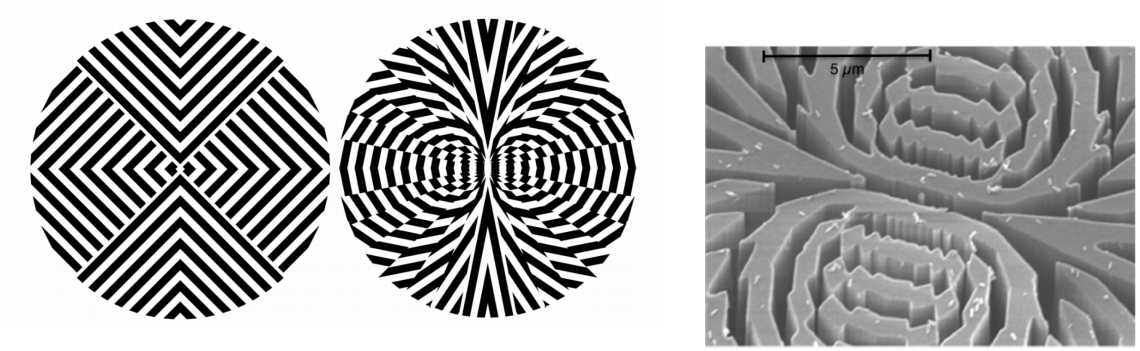

Figure 3. The two SGVC4 patterns manufactured in the past years. left: eight-segment, center: 32-segment straight lines design. right: SEM picture of the 32-segment SGVC4.[9] Only the central part is shown for clarity.

Only one of the masks (SGVC4-S32B) reached an acceptable rejection ratio* of around 600 over the full L band, which is comparable to the results obtained with an AGPM. SGVC4-S32A performs significantly worse although having the same pattern suggesting an anomaly in the fabrication process. It is not possible to conclude on the performance of the eight-segment mask SGVC4-S08 since only one mask has been manufactured and the poor performance can be due to manufacturing errors. The rejection ratios measured on VODCA are shown in table 1. The validity of the 32-segment straight lines pattern is confirmed with these results.

Table 1. Rejection ratio of the three manufactured masks. The performance is measured in one broadband (L-BBF: 3575nm-4125nm) and three narrowband filters (L-NBF1: 3425nm-3525nm, L-NBF2: 3710nm-3890nm, L-NBF3: 3960nm-4120nm) covering the astronomical L band.

	L-BBF	L-NBF1	L-NBF2	L-NBF3
SGVC4-S08	99	75	111	165
SGVC4-S32A	59	57	61	52
SGVC4-S32B	606	962	630	289

It is interesting to assess the performance of the SGVC4 in the presence of low order aberrations. On VODCA, we can add low order aberrations with a deformable mirror.[10] Tests on the sensitivity of the rejection ratio in presence of aberrations have been performed for an AGPM and the SGVC4. The results are shown in figure 4. The presence of tip/tilt and focus proves to have less influence on the performance of the SGVC4, which is expected from theory.[8]

When adding astigmatism, the figure of merit to calculate the rejection ratio needs to be adapted to the radial intensity profile of the attenuated PSF. Integrating up to 0.5 λ/D yields a counter-intuitive increase of the rejection ratio when adding astigmatism. The true rejection ratio is calculated including the first Airy ring, that is up to 2.23 λ/D (see figure 5). It is therefore crucial to know the radial profile of the PSF to correctly interpret the attenuation.

*Two equivalent metrics are used for assessing the performance of the SGVC: the null depth (as described in Ref. 2), and its inverse, the rejection ratio. We will use the rejection ratio throughout this paper.

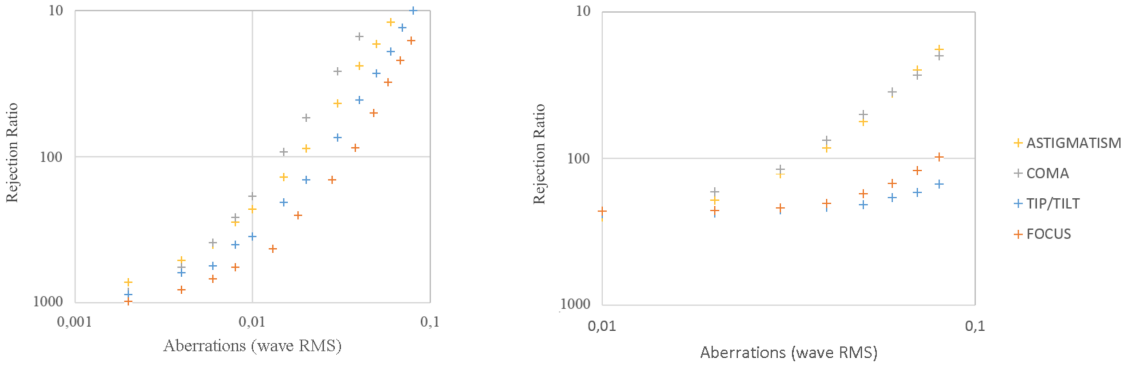

Figure 4. Influence of aberrations on the rejection ratio for the AGPM (left) and SGVC4 (right).

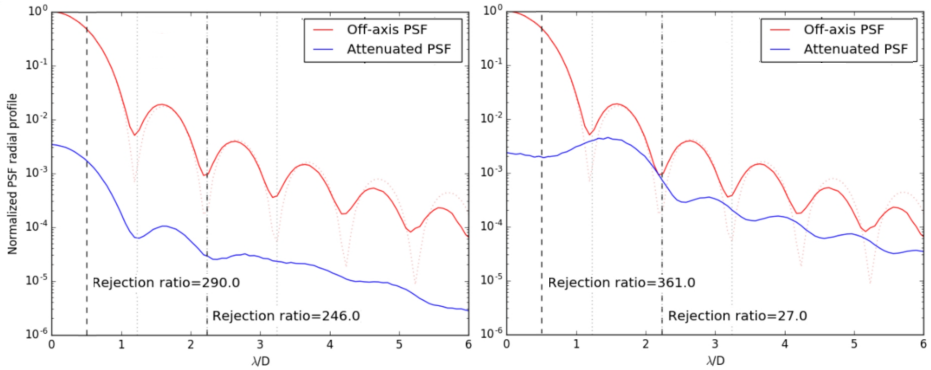

Figure 5. Influence of astigmatism on the attenuated PSF. Left: weak astigmatism, right: strong astigmatism. A sufficiently large ring needs to be included in the calculation of the rejection ratio to capture the effect of astigmatism.

The segmented design of the SGVC4 leaves its imprint on the transmitted light of an off-axis companion. Figure 6 shows the transmitted light of SGVC4-S32B as function of the position of the mask center. The mask is centered in the bottom left corner, where the rejection ratio is at its maximum. The off-axis transmission shows an intensity drop of 20 to 30% at the location of the transition between segments (there are eight segments in one quadrant). This means, that an already faint companion falling accidentally in these transition regions is attenuated by 20-30%. This is one of the main drawbacks of the segmented pattern and a reason to move on to study novel designs to produce the phase ramp.

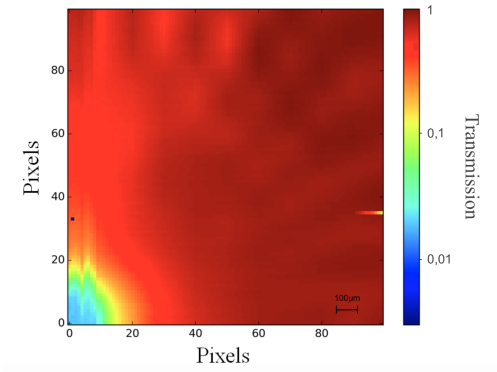

Figure 6. 2D map of off-axis transmission for SGVC4-S32B. The mask is centered at the bottom left.

4. FDTD SIMULATIONS

To develop new designs for vortex phase masks of topological charge 4 and higher we need to use a robust and versatile simulation tool. For designs based on subwavelength gratings a 2D RCWA[12] code is used to compute the grating parameters, which describes well an infinite parallel grating. While this condition is fulfilled approximately in the case of the AGPM (except for the central part of the mask), the absence of circular symmetry and the transition regions in the SGVC4 patterns urge us to use full 3D simulation tools. We use the rigorous FDTD code MEEP[13] to simulate those patterns.

We performed FDTD simulations for the AGPM including the central part (figure 7), which was not taken into account by our previous RCWA simulations. The results confirm that the RCWA results describe well the pattern when the grating lines are nearly parallel, while it breaks down at the center of the mask. The main leakage is resulting from the very central part of the AGPM where the curvature of the grating lines becomes considerable. The diagonal features are an artefact of the cartesian sampling of MEEP. The resulting phase ramp is well pronounced; the poor central part of the phase ramp arises from the non-parallel grating lines at the center of the mask.

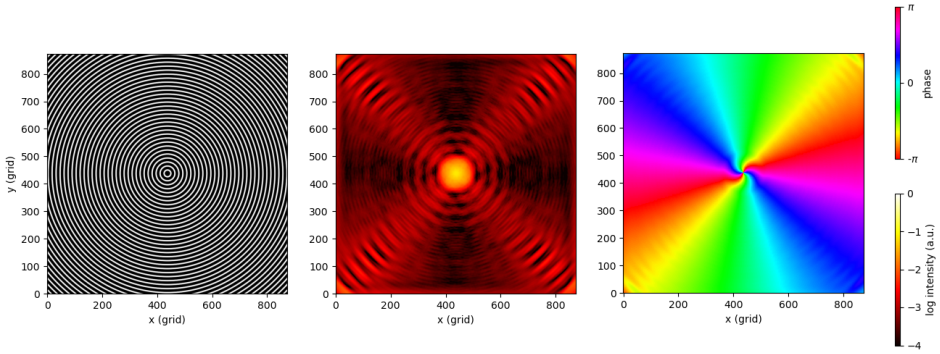

Figure 7. FDTD (MEEP) simulation of the central part of an AGPM (innermost 30 lines) showing (left) the grating pattern, (center) the leakage intensity and (right) the characteristic phase ramp.

Simulations were performed with the same FDTD code on three promising SGVC4 patterns. The two segmented designs introduced in Ref. 7 using straight and curved lines were used, as well as a third hybrid design combining curved lines along the x-axis and straight lines along the y-axis. The hybrid design avoids the unnecessary large number of segments encountered in both straight and curved lines designs. The three designs as well as the FDTD results are shown in figure 8. The hybrid design performs best (though all three patterns perform similarly), as expected since it combines the advantages of both straight and curved lines designs.

5. CONCLUSION

The manufactured SGVC4 masks have been assessed on the VODCA test bench confirming the 32-segments straight lines pattern. It is not possible to conclude on the eight-segments design. The drawbacks caused by the segmentation and the non-continuous phase ramp degrade the performance of the SGVC4, which is confirmed by FDTD simulations. An approach based on full metasurface patterns might be able to solve the problems encountered with subwavelength gratings in future. We are therefore investigating the possibility of creating the vortex effect using all-dielectric metasurfaces. Metasurfaces are a currently flourishing field of research and have proven to produce good quality vortex beams including all-dielectric designs.[14–19] Using single unit cells instead of relying on sectors of continuous grating patterns might avoid the degradation of the performance of our current charge 4 designs due to the transition regions between sectors. It is however important to achieve the degree of achromaticity required for astronomy applications. Exploiting the additional degrees of freedom of 2D metasurface structures might be able to satisfy these requirements.

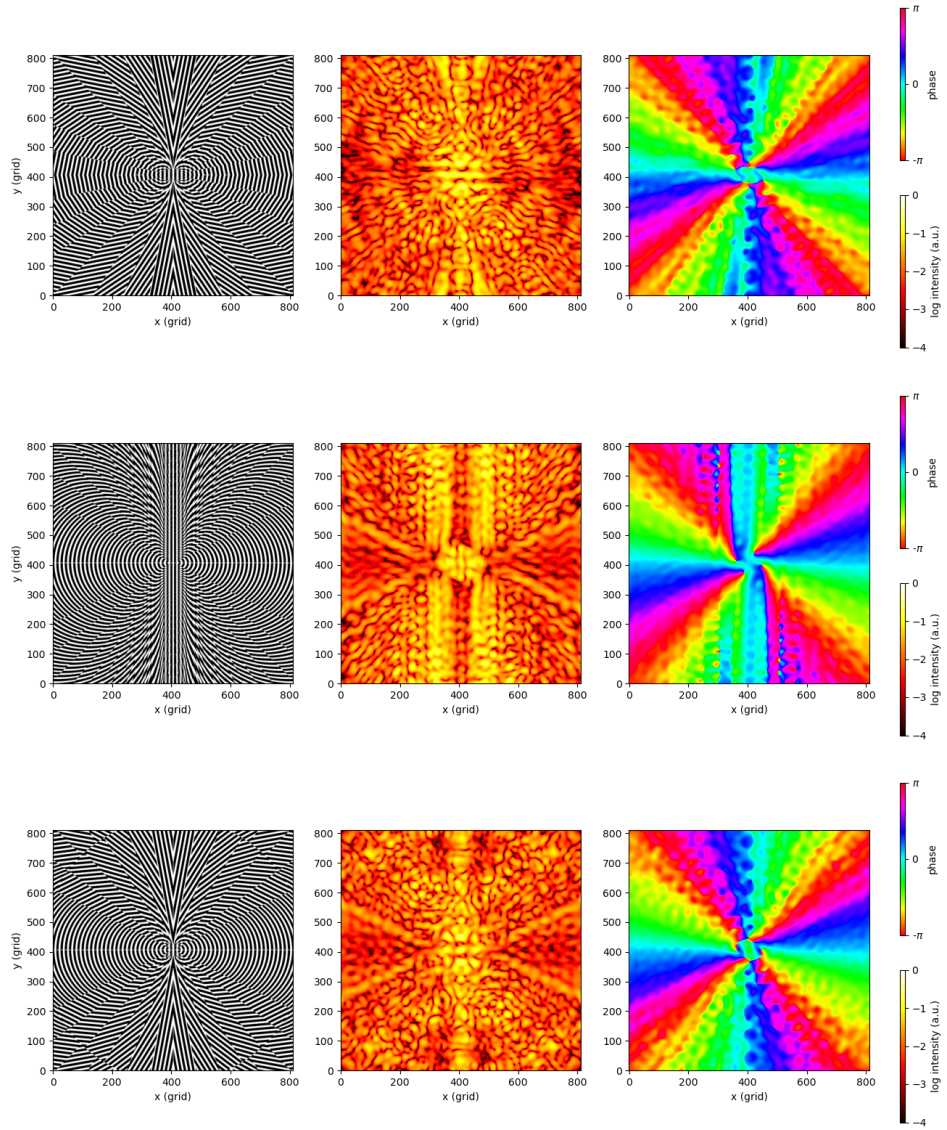

Figure 8. FDTD simulations with MEEP of three different charge-4 patterns: (a) straight lines, (b) curved lines and (c) hybrid design. The images show (left) the grating pattern, (middle) the leakage intensity and (right) the characteristic phase ramp.

ACKNOWLEDGMENTS

This project has received funding from the European Research Council (ERC) under the European Union's Horizon 2020 research and innovation programme (grant agreement No 819155).

REFERENCES

[1] Schneider, J., Dedieu, C., Le Sidaner, P., Savalle, R., and Zolotukhin, I., "Defining and cataloging exoplanets: the exoplanet.eu database," *A&A* **532**, A79 (2011). `exoplanet.eu` accessed 30 November 2020.

[2] Mawet, D., Riaud, P., Absil, O., and Surdej, J., "Annular Groove Phase Mask Coronagraph," *ApJ* **633**(2), 1191–1200 (2005).

[3] Delacroix, C., Absil, O., Mawet, D., Hanot, C., Karlsson, M., Forsberg, P., Pantin, E., Surdej, J., and Habraken, S., "A diamond AGPM coronagraph for VISIR," in [*Ground-based and Airborne Instrumentation for Astronomy IV*], McLean, I. S., Ramsay, S. K., and Takami, H., eds., *Proc. SPIE* **8446**, 84468K (2012).

[4] Mawet, D., Absil, O., Delacroix, C., Girard, J. H., Milli, J., O'Neal, J., Baudoz, P., Boccaletti, A., Bourget, P., Christiaens, V., Forsberg, P., Gonte, F., Habraken, S., Hanot, C., Karlsson, M., Kasper, M., Lizon, J. L., Muzic, K., Olivier, R., Peña, E., Slusarenko, N., Tacconi-Garman, L. E., and Surdej, J., "L'-band AGPM vector vortex coronagraph's first light on VLT/NACO. Discovery of a late-type companion at two beamwidths from an F0V star," *A&A* **552**, L13 (2013).

[5] Absil, O., Milli, J., Mawet, D., Lagrange, A. M., Girard, J., Chauvin, G., Boccaletti, A., Delacroix, C., and Surdej, J., "Searching for companions down to 2 AU from β Pictoris using the L'-band AGPM coronagraph on VLT/NACO," *A&A* **559**, L12 (2013).

[6] Defrère, D., Absil, O., Hinz, P., Kuhn, J., Mawet, D., Mennesson, B., Skemer, A., Wallace, K., Bailey, V., Downey, E., Delacroix, C., Durney, O., Forsberg, P., Gomez, C., Habraken, S., Hoffmann, W. F., Karlsson, M., Kenworthy, M., Leisenring, J., Montoya, M., Pueyo, L., Skrutskie, M., and Surdej, J., "L'-band AGPM vector vortex coronagraph's first light on LBTI/LMIRCam," in [*Adaptive Optics Systems IV*], Marchetti, E., Close, L. M., and Vran, J.-P., eds., *Proc. SPIE* **9148**, 91483X (2014).

[7] Delacroix, C., Absil, O., Carlomagno, B., Piron, P., Forsberg, P., Karlsson, M., Mawet, D., Habraken, S., and Surdej, J., "Development of a subwavelength grating vortex coronagraph of topological charge 4 (SGVC4)," in [*Ground-based and Airborne Instrumentation for Astronomy V*], Ramsay, S. K., McLean, I. S., and Takami, H., eds., *Proc. SPIE* **9147**, 91478Y (2014).

[8] Huby, E., Baudoz, P., Mawet, D., and Absil, O., "Post-coronagraphic tip-tilt sensing for vortex phase masks: The QACITS technique," *A&A* **584**, A74 (2015).

[9] Vargas Catalán, E., Piron, P., Jolivet, A., Forsberg, P., Delacroix, C., Huby, E., Absil, O., Vartiainen, I., Kuittinen, M., and Karlsson, M., "Subwavelength diamond gratings for vortex coronagraphy: towards an annular groove phase mask for shorter wavelengths and topological charge 4 designs," *Opt. Mater. Express* **8**(7), 1976–1987 (2018).

[10] Jolivet, A., Orban de Xivry, G., Huby, E., Piron, P., Catalan, E. V., Habraken, S., Surdej, J., Karlsson, M., and Absil, O., "L- and M-band annular groove phase mask in lab performance assessment on the vortex optical demonstrator for coronagraphic applications," *J. Astron. Telesc. Instrum. Syst.* **5**, 025001 (2019).

[11] Jolivet, A., *Development and exploitation of an infrared coronagraphic test bench for vortex phase mask performance assessment*, PhD thesis, University of Liège (2019).

[12] Moharam, M. G. and Gaylord, T. K., "Diffraction analysis of dielectric surface-relief gratings," *J. Opt. Soc. Am.* **72**(10), 1385–1392 (1982).

[13] Oskooi, A. F., Roundy, D., Ibanescu, M., Bermel, P., Joannopoulos, J. D., and Johnson, S. G., "MEEP: A flexible free-software package for electromagnetic simulations by the FDTD method," *Comput. Phys. Commun.* **181**(3), 687–702 (2010).

[14] Chen, W. T., Zhu, A. Y., and Capasso, F., "Flat optics with dispersion-engineered metasurfaces," *Nat. Rev. Mater.* **5**, 604–620 (2020).

[15] Devlin, R. C., Ambrosio, A., Rubin, N. A., Mueller, B., and Capasso, F., "Arbitrary spin-to-orbital angular momentum conversion of light," *Science* **358**(6365), 896–900 (2017).

[16] Zhan, A., Colburn, S., Trivedi, R., Fryett, T. K., Dodson, C. M., and Majumdar, A., "Low-contrast dielectric metasurface optics," *ACS Photonics* **3**(2), 209–214 (2016).

[17] Devlin, R. C., Ambrosio, A., Wintz, D., Oscurato, S. L., Zhu, A. Y., Khorasaninejad, M., Oh, J., Maddalena, P., and Capasso, F., "Spin-to-orbital angular momentum conversion in dielectric metasurfaces," *Opt. Express* **25**(1), 377–393 (2017).

[18] Shalaev, M. I., Sun, J., Tsukernik, A., Pandey, A., Nikolskiy, K., and Litchinitser, N. M., "High-efficiency all-dielectric metasurfaces for ultracompact beam manipulation in transmission mode," *Nano Letters* **15**(9), 6261–6266 (2015).

[19] Chong, K. E., Staude, I., James, A., Dominguez, J., Liu, S., Campione, S., Subramania, G. S., Luk, T. S., Decker, M., Neshev, D. N., Brener, I., and Kivshar, Y. S., "Polarization-independent silicon metadevices for efficient optical wavefront control," *Nano Letters* **15**(8), 5369–5374 (2015).